Article ID: 1003－6326(2005)01－0064－08

Finite element polycrystal model simulation of cold rolling textures in deformation processed two-phase Nb/Al metal-metal composites①

CHEN Li-qing(陈礼清)[1, 2], KANETAKE Naoyuki[2]
(1. Institute of Metal Research, Chinese Academy of Sciences, Shenyang 110016, China;
2. School of Engineering, Nagoya University, Furo-cho, Chikusa-ku, Nagoya 464-8603, Japan)

Abstract: The finite element polycrystal model (FEPM) was extended and applied to simulate the development of the cold rolling textures of matrix aluminum in deformation processed two-phase 10% and 20% Nb/Al(in volume fraction) metal-metal composites on the basis of slip deformation of individual grains. This simulation method can assure the continuity of stress and displacement at the boundary during heterogeneous deformation and take arbitrary boundary conditions into consideration. The starting hot-extruded textures, as initial input condition, were taken into account in the FEPM simulation. The simulation results show that the main texture components and their evolution after various cold rolling reductions in 10% and 20% Nb/Al metal-metal composites are well qualitatively in agreement with the experimental ones. The initially extruded textures are rather weak, so they have no much influence on the simulated final cold rolling textures of the matrix aluminum for Nb/Al composites.

Key words: metal-matrix composites; FEPM; Nb/Al composite; texture; rolling
CLC number: TB331, TG335.8 **Document code:** A

1 INTRODUCTION

Due to the combination of excellent electrical and thermal conductivity and high ultimate tensile strength, the deformation processed two-phase metal-metal composites have long been the interests of materials scientists and physical metallurgists[1-3]. Till now, there are many experimental investigations on fabricating, mechanical properties, physical behavior and strengthening mechanisms for this kind of composites produced in the form of wires[4-7]. However, there are limited reports on the sheet metal-metal composites.

For large particulate reinforced Nb/Al deformation processed sheet metal-metal composites, the manufacturing process and mechanical behavior[8], textural evolution analysis during hot extrusion and cold rolling process[9, 10] were carried out in order to explore the strengthening mechanism associated with texture. It was revealed that the matrix plastic deformation would be affected by the large second phase particulate existing within the composites to some extent and the cold rolled texture exhibited a little difference from the typical FCC β-fiber, which could be represented by main components as B-{011}⟨211⟩, S′-{124}⟨654⟩ and C′-{113}⟨332⟩.

As we all know, the classic Taylor approach, Sachs model and several modified models can be utilized to simulate the cold rolling texture development. However, the advantages of the present finite element polycrystal model (FEPM) lies in the following three aspects. Firstly, it can assure the continuity of the stress and displacement at the boundary during heterogeneous deformation of materials. Secondly, the arbitrary boundary conditions could be taken into consideration in this model. Finally, one can conduct the calculation of the individual grain rotation and deformation behavior under any loading paths. This method is originally developed for calculation of the plastic deformation behavior and texture changes in pure metals[11-16]. Takahashi et al[14-16] conducted many calculations on the deep-drawability and mechanical properties and revealed that the FEPM has a potential to disclose the essentials in particulate related two-phase materials.

In this paper, we mainly focused on the theoretical calculation of the cold rolling texture evolution of matrix Al in Nb/Al metal-metal composites based on the finite element method (FEM) and polycrystalline plastic deformation theory. The FEPM approach in this study was further developed so as to adapt to the simulation of the cold rolling texture evolution for powder metallurgy (PM) processed 10% and 20% Nb/Al(in volume

① **Received date:** 2004－06－02; **Accepted date:** 2004－11－04
Correspondence: CHEN Li-qing, Associate professor, PhD; Tel: +86-24-83978245; Fax: +86-24-23891320;
E-mail address: lqchen@imr.ac.cn

fraction) two-phase metal-metal composites, where the initial hot-extruded textures were taken into consideration in this model. A comparison and discussion were also made between the calculated and experimental results.

2 MODEL DESCRIPTION

As shown in Fig. 1, the number of the cubic finite elements was set as $6 \times 6 \times 6 = 216$ in this model and the stacking way is arranged as in Fig. 1 (a). Each cubic element represents a grain with certain initial Euler angles $\{\varphi_1, \Phi, \varphi_2\}$.

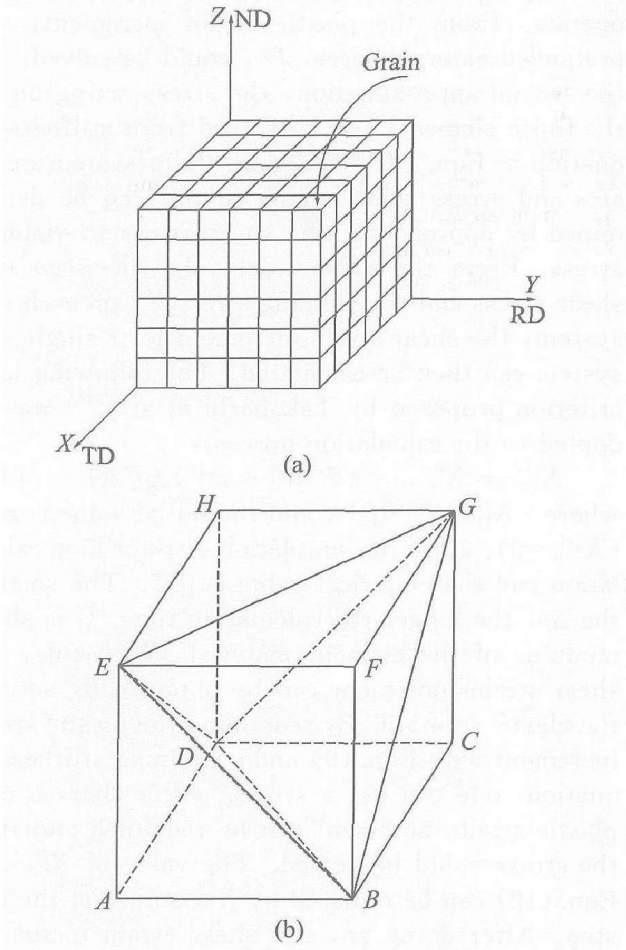

Fig. 1 Schematic diagram of FEPM
(a) —Stacking way of finite elements;
(b) —One way of dividing element required by FEM
(ND—Normal direction; RD—Rolling direction;
TD—Transverse direction)

For 10% and 20% Nb/Al metal-metal composites, the number of the second phase Nb particulates and their arrangement in the model were predetermined as in Fig. 2. X, Y and Z represent the sample's transverse (TD), rolling (RD) and normal directions (ND), respectively. Generally, it is reasonable to regard a rolling deformation as plane-strain compressive deformation behavior where the strain in the transverse direction is forbidden. Within the framework of FEM, each cubic finite element could be divided into 5 pyramids in order to establish the relationship between node's stress and displacement, and in such a case there are two ways of division, which would be all taken into the calculation. Fig. 1(b) shows one way of dividing such an element.

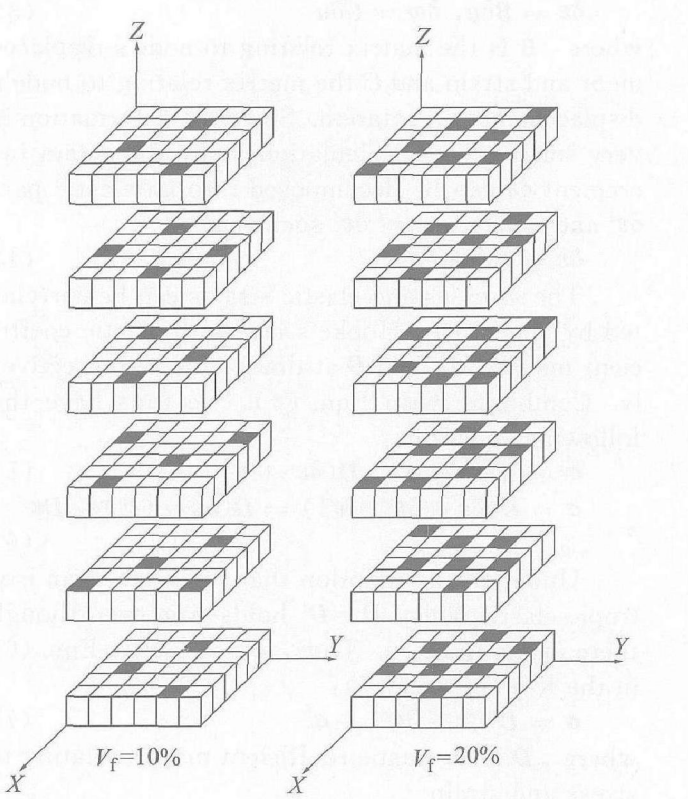

Fig. 2 Distribution of reinforcement particulates in Nb/Al composites employed in FEPM
(Black blocks—Nb particulates)

The final grain orientation in Euler angles, $\{\varphi_1, \Phi, \varphi_2\}$, can be represented by initial orientation $\{\varphi_{01}, \Phi_0, \varphi_{02}\}$ and orientation change, $\{\Delta\varphi_{k1}, \Delta\Phi_k, \Delta\varphi_{k2}\}$, over all the simulated deformation steps, n, as follows:

$$\{\varphi_1, \Phi, \varphi_2\} = \{\varphi_{01}, \Phi_0, \varphi_{02}\} + \sum_{k=1}^{n} \{\Delta\varphi_{k1}, \Delta\Phi_k, \Delta\varphi_{k2}\} \quad (1)$$

The initial Euler angles $\{\varphi_{01}, \Phi_0, \varphi_{02}\}$ of the grains can be calculated from the experimentally measured pole figure data with the method proposed by Takahashi[17]; while the orientation change at each deformation step k, $\{\Delta\varphi_{k1}, \Delta\Phi_k, \Delta\varphi_{k2}\}$, could be calculated on the basis of FEM in combination with the principle of virtual work. The details can be described as follows.

Let us consider a grain with surface area of S and volume V, on which the unit surface tension is T_i. The displacement, stress and strain at time t_1 are denoted as u_i, σ_{ij} and ε_{ij}, respectively. Neglecting the volumetric force, the expression for the virtual work could be written as Eqn. (2) after this grain underwent a deformation or had an incremental strain $\delta\varepsilon_{ij}$ from time t_1 to t.

$$\delta\Phi = \int_V (\sigma_{ij}\,\delta\varepsilon_{ij})\,dV - \int_S (T_i\,\delta u_i)\,dS = 0 \quad (2)$$

At this time, the incremental strain and spin tensors may be written with incremental displacement tensor in the form of matrix:

$$\delta\varepsilon = \boldsymbol{B}\delta\boldsymbol{u},\quad \delta\omega = \boldsymbol{C}\delta\boldsymbol{u} \quad (3)$$

where $\boldsymbol{B}$ is the matrix relating to node's displacement and strain and $\boldsymbol{C}$ the matrix relating to node's displacement and rotation. Since the deformation is very small at each calculation step, the strain increment $\delta\varepsilon$ can be decomposed into an elastic part $\delta\varepsilon^e$ and a plastic part $\delta\varepsilon^p$ such that

$$\delta\varepsilon = \delta\varepsilon^e + \delta\varepsilon^p \quad (4)$$

The stresses and elastic strains can be correlated by generalized Hooke's law with elastic coefficient matrices $\boldsymbol{D}^1$ and $\boldsymbol{D}$ at time t_1 and t, respectively. Combining with Eqn. (4), we thus have the following equations:

$$\sigma^1 = \boldsymbol{D}^1\varepsilon^{e1},\quad \sigma = \boldsymbol{D}(\delta\varepsilon^e + \varepsilon^{e1}) \quad (5)$$

$$\sigma = \boldsymbol{D}(\delta\varepsilon - \delta\varepsilon^p + \varepsilon^{e1}) = \boldsymbol{D}(\delta\varepsilon - \delta\varepsilon^p) + \boldsymbol{D}\varepsilon^{e1} \quad (6)$$

Under the assumption that the grain is an isotropic elastic body, $\boldsymbol{D} = \boldsymbol{D}^1$ holds true even though there exists rotation. Thus, we can write Eqn. (6) in the form of Eqn. (7):

$$\sigma = \boldsymbol{D}(\delta\varepsilon - \delta\varepsilon^p) + \sigma^1 \quad (7)$$

where $\boldsymbol{D}$ is an elastic coefficient matrix relating to stress and strain.

Substituting Eqns. (3) and (7) into Eqn. (2), the stiffness Eqn. (8) of FEM can be obtained:

$$\boldsymbol{K}\delta\boldsymbol{u} = \boldsymbol{F} + \boldsymbol{F}^p \quad (8)$$

where $\boldsymbol{K} = \int \boldsymbol{B}^{\mathrm{T}}\boldsymbol{D}\boldsymbol{B}\,dV$, $\boldsymbol{F}^p = \int \boldsymbol{B}^{\mathrm{T}}(\boldsymbol{D}\delta\varepsilon^p - \sigma^1)\,dV$, and means the pretended external force on the nodes. Once the plastic strain increment $\delta\varepsilon^p$ is determined, the value of $\boldsymbol{F}$, force on the nodes, could be obtained. The solving process was established on the basis of crystal plasticity theory.

Within the crystal plasticity framework, plastic deformation is viewed in term of slip of crystallographic planes and a phenomenological relation for the shear strain along each of the slip systems. The slip of crystallographic planes on the r-th slip system for an element is defined by their normal unit $a_i^{(r)}$ and slip direction $b_i^{(r)}$. In such a case, if the shear strain increment in an element is denoted as $\delta\gamma^{(r)}$, and then the plastic strain increment $\delta\varepsilon_{ij}^p$ and spin increment $\delta\omega_{ij}^p$ can be expressed as

$$\delta\varepsilon_{ij}^p = \sum L_{ij}^{(r)}\,\delta\gamma^{(r)},\quad \delta\omega_{ij}^p = \sum W_{ij}^{(r)}\,\delta\gamma^{(r)} \quad (9)$$

where $L_{ij}^{(r)} = (a_i^{(r)}b_j^{(r)} + a_j^{(r)}b_i^{(r)})/2$, and $W_{ij}^{(r)} = (a_i^{(r)}b_j^{(r)} + a_j^{(r)}b_i^{(r)})/2$. The shear stress working on each of the slip system should be

$$\tau = L_{ij}^{(r)}\sigma_{ij} \quad (10)$$

If the yielding shear stress on the slip systems is $k^{(r)}$, the yielding condition can be written as

$$\xi^{(r)}\tau^{(r)} = k^{(r)},\quad \xi^{(r)}\delta\gamma^{(r)} > 0$$

$$\xi^{(r)}\tau^{(r)} < k^{(r)},\quad \xi^{(r)}\delta\gamma^{(r)} = 0 \quad (11)$$

where $\xi^{(r)} = \mathrm{sign}(\tau^{(r)})$ is a sign function.

Generally, it is hard to determine which slip system is active to slip. Here we introduced the loop criterion proposed by Takahashi to the calculation process according to the practical deformation path, and the details can be found in Refs. [14, 16, 17]. As the first approximation, the plastic strain increment after first deformation step is viewed as elastic strain, thus the plastic increment is zero. On the basis of the elastic solution, if the shear stresses on the slip systems exceed the yielding stress, there will be some slip systems to operate. From the plastic strain increment, the pretended external force, F^p, could be solved. As the second approximation, the stress acting on all the finite elements can be solved from stiffness equation in Eqn. (8). Whether a slip system operates and stress relief occurs or not can be determined by approaching the shear stress to yielding stress. From the differential value between this shear stress and the yielding stress $k^{(r)}$ on each slip system, the shear strain increment for a single slip system can then be calculated. The following loop criterion proposed by Takahashi et al[14, 16] was adopted to the calculation process:

$$X_{(i)}^{(r)} = X_{(i-1)}^{(r)} + (\xi^{(r)}\tau^{(r)} - k^{(r)})\,\Delta\rho/2G \quad (12)$$

where $X_{(i)}^{(r)} = \xi^{(r)}\delta\gamma^{(r)}$, and the initial value is zero ($X_{(0)}^{(r)} = 0$). $\Delta\rho$ is the simulation step for loop calculation and the empirical value is 0.5. The smaller the $\Delta\rho$, the longer the calculating time. G is shear modulus of the element material. With this, the shear strain increment can be obtained by solving the elastic solution. By redefining the plastic strain increment with Eqn. (9) and combining stiffness equation, one can get a stress. After that, a new plastic strain increment can be redefined and then the stress could be solved. The value of $X_{(i-1)}^{(r)}$ in Eqn. (12) can be replaced by $X_{(i)}^{(r)}$ solved at the last step. After doing so, the shear strain increment can be calculated as shear stress approaches the yielding stress. By utilizing Eqn. (9), the plastic spin increment of the grain can be computed.

It is reasonable to neglect the elastic deformation when the grains undergo large plastic deformation, and the spin tensor can then be described as

$$\delta\omega_{ij}^* = \delta\omega_{ij} - \delta\omega_{ij}^p \quad (13)$$

Based on the above equation, the change of Euler angles $\{\Delta\varphi_1,\ \Delta\phi,\ \Delta\varphi_2\}$ for representing the grain orientation during deformation process can be obtained by utilizing coordinate transformation in Euler space. The pole figure for any crystal plane can then be plotted where the orientation is denoted by discrete dots due to limited number of elements.

Table 1 lists the materials parameters necessary for calculating the deformation texture for Nb/

Al composites with FEPM approach. Since the second phase particulates Nb were hardly deformed at extruded state and the orientation distribution of the Nb is nearly random, the initial texture of the particulate Nb was reasonably assumed to be randomly distributed over the whole Euler space. Thus, the Euler angles for the second-phase Nb particulates shown in Fig. 2 were randomly generated according to the following equations:

$$\varphi_1 = 2\pi \cdot \mathrm{ran}(i)$$
$$\Phi = \arccos[1 - 2\mathrm{ran}(i)]$$
$$\varphi_2 = 2\pi \cdot \mathrm{ran}(i) \quad (14)$$

Table 1 Parameters used in simulation

Component	Slip system	Shear modulus/GPa	Elastic modulus/GPa	Poisson ratio
Al	12{111}⟨110⟩	26	70	0.33
Nb	12{110}⟨111⟩	56	149	0.33

where ran(i) takes randomly distributed numbers between 0 and 1 for i-th grains in order to meet the requirements of Euler angles' range.

There are 12 equivalent {111}⟨110⟩ slip systems for Al and also 12 equivalent {110}⟨111⟩ slip systems for Nb selected for calculation in this model.

3 RESULTS AND DISCUSSION

For comparison, we used and presented the pole figures recalculated from the ODFs and those from simulated ones in discretionized pole figures obtained by random sampling method[17], since the recalculated pole figures from ODFs are of high symmetry and avoid the untrue part caused by experimental factors. The composites processing, texture measurement and ODFs calculation details for 10% and 20% Nb(volume fraction)/Al metal-metal composites can be found in Refs. [9, 10, 19].

In order to readily analyze the texture components and evolution process, we depicted some ideal orientation locations in a {200} pole figure for cold-rolled FCC structural metals shown in Fig. 3.

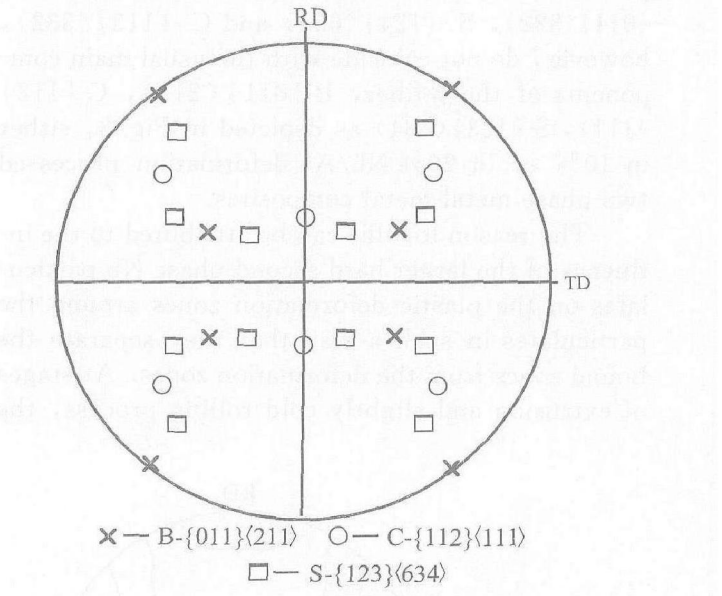

Fig. 3 Some important ideal orientations of rolled FCC metals in {200} pole figure

3.1 Starting or extruded textures

Figs. 4 and 5 show the recalculated results and their corresponding discrete pole figures for 10% and 20% Nb/Al metal-metal composites extruded at 500 ℃, respectively. Since the volume fraction of second phase particulate Nb in Fig. 4 is 10% and lower than that in Fig. 5, and it displays somewhat stronger extruded textures within the matrix aluminum. As a whole, the textures at extruded states are weak and no sharp textures exist within

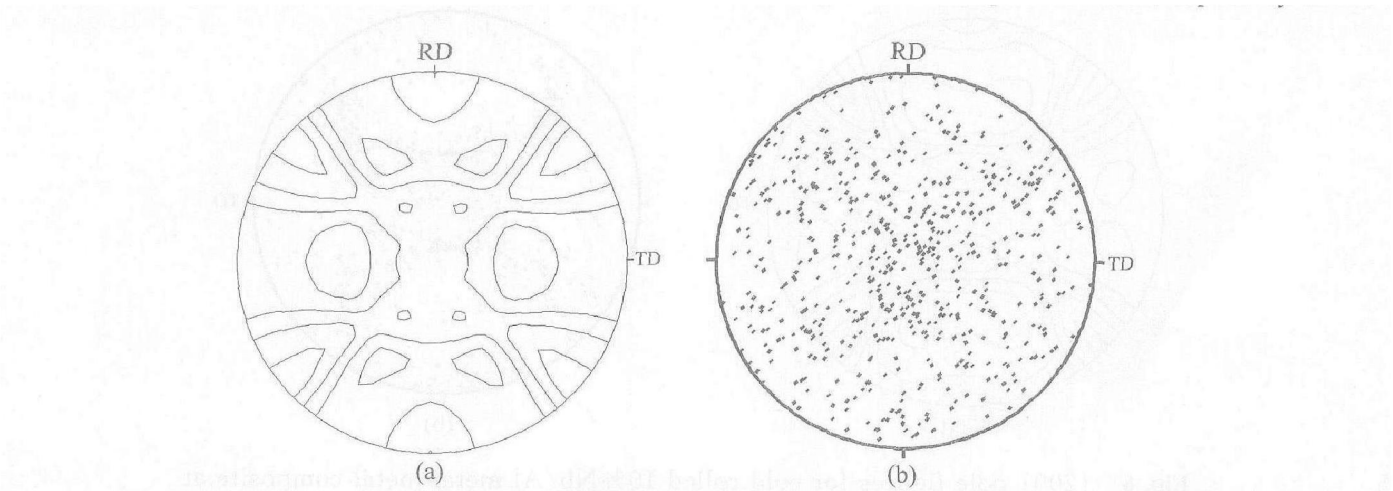

Fig. 4 {200} pole figures for flat extruded 10% Nb/Al metal-metal composite
(a) —{200} pole figure recalculated from ODFs; (b) —Discrete {200} pole figure corresponding to (a)
(Intensity levels in (a): 0.5, 1.0, 1.5, ···)

the matrix of the composites. Randomly distributed component takes predominant, especially in the case for 20% Nb/Al. The discrete pole figures display subtly preferred orientations similar to its corresponding pole figures.

The hot extruded textures were experimentally measured and analyzed in Ref. [10] and it indicates that the flat extruded textures in such a case are similar to those of the cold rolled textures of pure FCC metals. Some main orientations, B′-{011}⟨322⟩, S′-{124}⟨654⟩ and C′-{113}⟨332⟩, however, do not coincide with the usual main components of the β-fiber, B-{011}⟨211⟩, C-{112}⟨111⟩, S-{123}⟨634⟩ as depicted in Fig. 3, either in 10% or in 20% Nb/Al deformation processed two-phase metal-metal composites.

The reason for this can be attributed to the influence of the larger hard second-phase Nb particulates on the plastic deformation zones around the particulates in such a way that they separate the bound zones from the deformation zones. At stages of extrusion and slightly cold rolling process, the massively bound zones within composites remain and the weak textures slightly deviating from the standard β-fiber are produced. In both cases of 10% and 20% Nb/Al, the textural characteristic behaves the same and can be featured as weak β-fibers where the main texture components all mainly consist of B′-{011}⟨322⟩, S′-{124}⟨654⟩ and C′-{113}⟨332⟩, as shown in Figs. 4–7.

3.2 Cold rolling textures

Although the simulated and experimentally measured textures for extruded and cold rolled up to 50% Nb/Al metal-metal composites are weak and consist mainly of B′-{011}⟨322⟩, S′-{124}⟨654⟩ and C′-{113}⟨332⟩, the case is different from that under severe cold rolling reductions. For the 10% and 20% Nb/Al metal-metal composites under much heavy cold rolling reduction, the texture characteristics can be comparatively observed in Figs. 6–9.

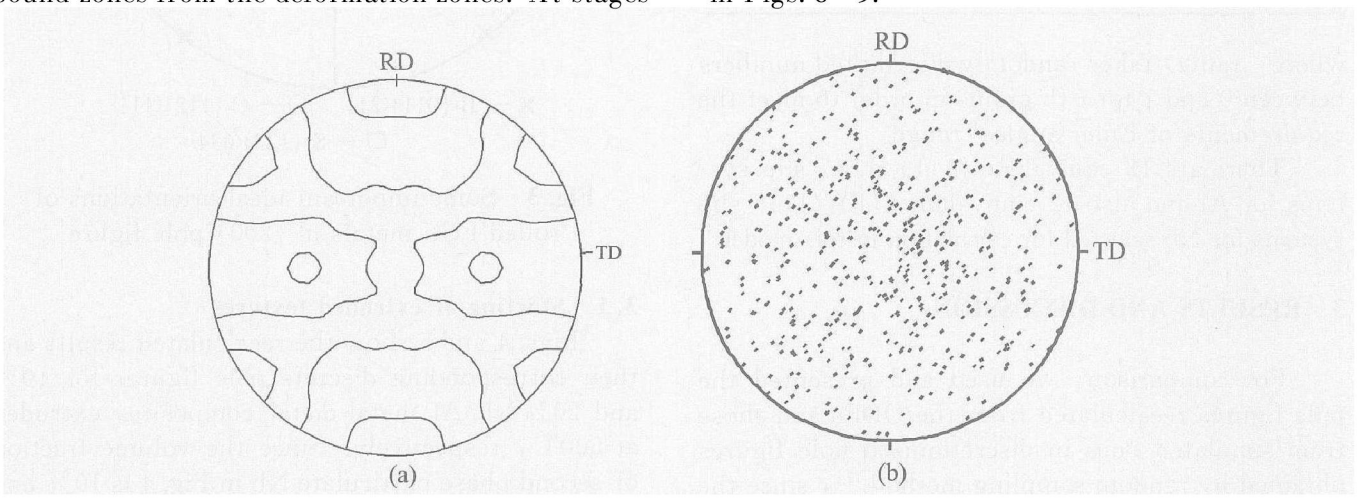

Fig. 5 {200} pole figures for flat extruded 20% Nb/Al metal-metal composite
(a) —{200} pole figure recalculated from ODFs; (b) —Discrete {200} pole figure corresponding to (a)
(Intensity levels in (a): 0.5, 1.0, 1.5, …)

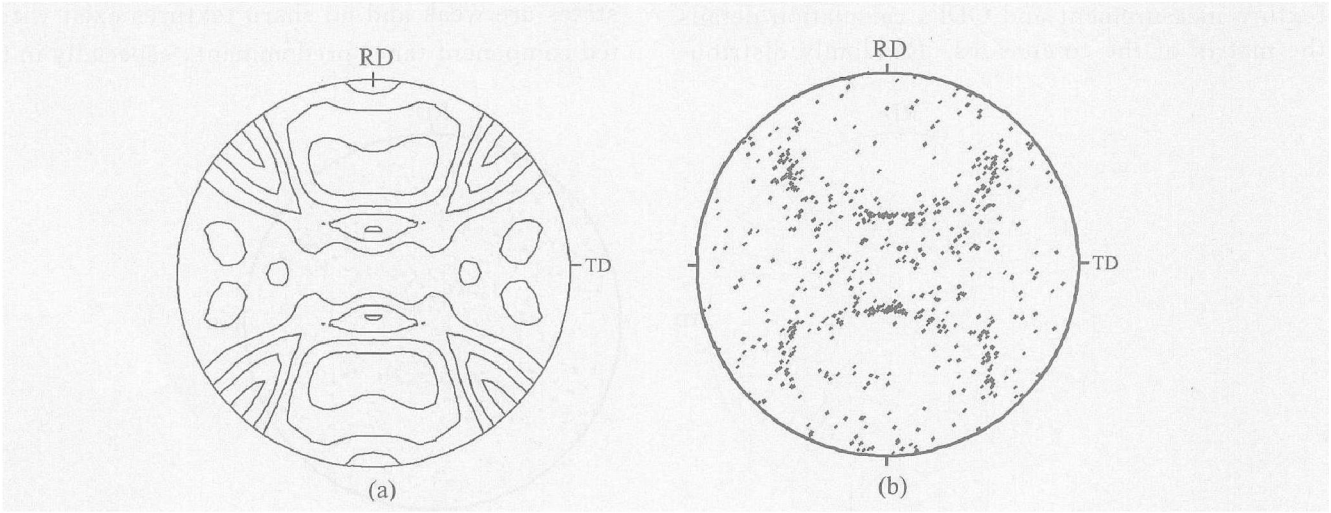

Fig. 6 {200} pole figures for cold rolled 10% Nb/Al metal-metal composite at 50% cold rolling reduction
(a) —{200} pole figure recalculated from ODFs; (b) —Simulated discrete {200} pole figure
(Intensity levels in (a): 0.5, 1.0, 1.5, …)

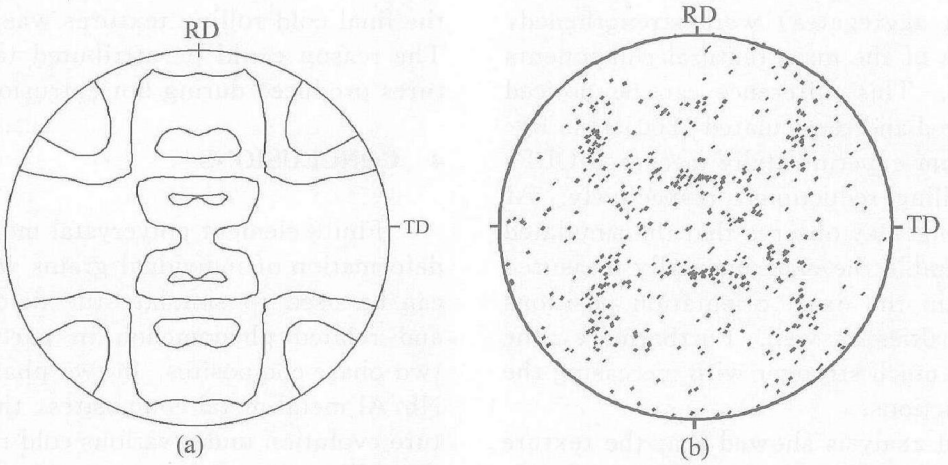

Fig. 7 {200} pole figures for cold rolled 20% Nb/Al metal-metal composite at 50% cold rolling reduction

(a) —{200} pole figure recalculated from ODFs; (b) —Simulated discrete {200} pole figure (Intensity levels in (a): 0.5, 1.0, 1.5, ...)

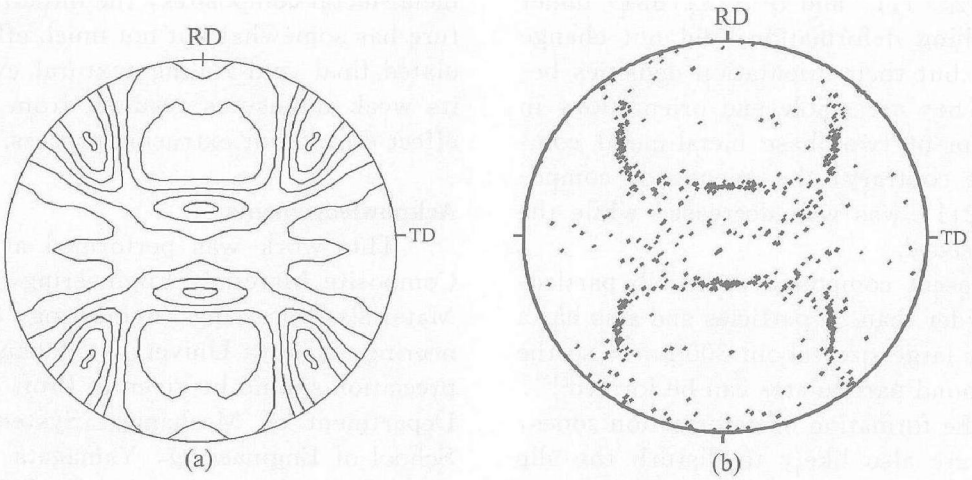

Fig. 8 {200} pole figures for cold rolled 10% Nb/Al metal-metal composite at 80% cold rolling reduction

(a) —{200} pole figure recalculated from ODFs; (b) —Simulated discrete {200} pole figure (Intensity levels in (a): 0.5, 1.0, 1.5, ...)

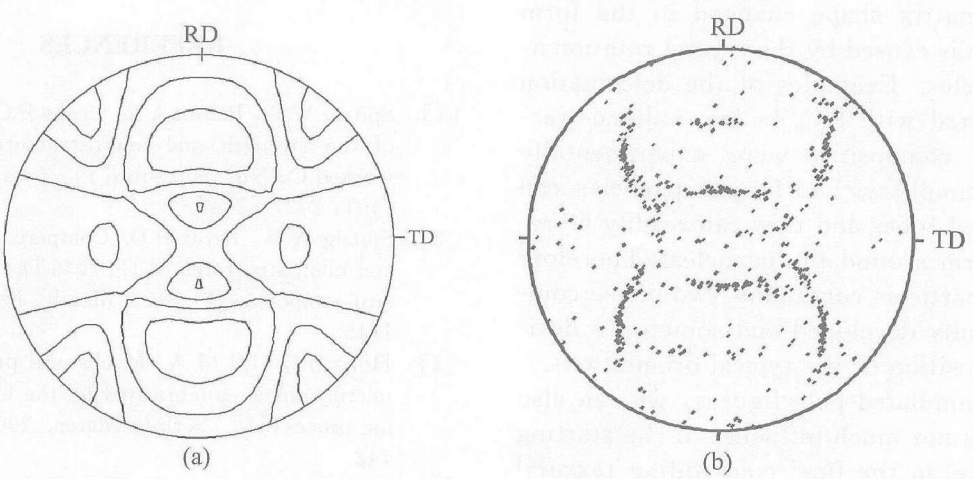

Fig. 9 {200} pole figures for cold rolled 20% Nb/Al metal-metal composite at 80% cold rolling reduction

(a) —{200} pole figure recalculated from ODFs; (b) —Simulated discrete {200} pole figure (Intensity levels in (a): 0.5, 1.0, 1.5, ...)

In Figs. 8 and 9, not only the texture intensities (revealed as dot aggregates) were strengthened, but the positions of the main textural components changed as well. This difference can be noticed from the simulated and recalculated {200} pole figures obtained from experimentally measured ODFs at 80% cold rolling reductions, respectively. At the same time, one may observe that the simulated pole figures resemble the experimentally measured ones, not only in the exact orientation positions but in the intensities as well. Furthermore, the textures become much stronger with increasing the cold rolling reductions.

The detailed analysis showed that the texture components of B′-{011}〈322〉 gradually transformed towards the B-{011}〈211〉 when heavy cold rolling reduction were exerted on the composites, as shown in Figs. 8 and 9. The other components, such as C′-{113}〈332〉 and S′-{124}〈654〉, which is near to C-{112}〈111〉 and S-{123}〈634〉 under further cold rolling deformation, did not change their locations, but their orientation densities become higher. They are stable end orientations in matrix aluminum of two-phase metal-metal composites. On the contrary, the orientation component B-{011}〈211〉 was well decreased while the simulation proceeded.

For the present composites, the Nb particulate is much harder than Al particles and also has a relatively rather large size (about 300 μm), so the bound zones around particulates can be formed[10]. In addition to the formation of deformation zones, large particles are also likely to disturb the slip pattern in the matrix, resulting in a lensoid distortion of the substructure around the particle. A lensoid distortion of the substructure generally originates from the inhomogeneous deformation in matrix by multi-slip around the large particles with the periphery matrix shape changed in the form like lens, which is caused by the crystal rotation around the particles. Examples of the deformation features associated with SiC_p in low volume fraction aluminum composites were experimentally provided by Humphreys[18]. Larger particles can produce distorted zones and they can readily be restricted to deform around the particles. Therefore the texture in particles containing two-phase composites is not fully developed and sometimes deviates from the position of the typical orientations.

From the simulated pole figures, we can also see that there is not much influence of the starting extruded texture on the final cold rolling textural evolution in Nb/Al metal-metal composites. However, during the primary stage of cold rolling, the cold rolled texture is predominantly determined by the extruded textures. The simulation was also conducted for randomly distributed starting orientations in 20% Nb/Al composite and revealed that the final cold rolling textures was rather alike[19]. The reason could be attributed to the weak textures produced during hot extrusion process.

4 CONCLUSIONS

Finite element polycrystal model based on slip deformation of individual grains was extended and can be used to simulate the deformation texture and related phenomenon in particulate-contained two-phase composites. In two-phase 10% and 20% Nb/Al metal-metal composites, the simulated texture evolution under various cold rolling reductions are well qualitatively in agreement with the experimental results. It is the hard Nb particulates in Nb/Al composites that restrict the plastic deformation and separate the deformation zones from the bound zones around the particulates. For Nb/Al metal-metal composites, the initially extruded texture has somewhat but not much effect on the simulated final cold rolling textural evolution due to its weak intensities resulted from the particulate effect during hot extrusion process.

Acknowledgements

This work was performed at Laboratory of Composite Materials Engineering, Department of Materials Processing Engineering, School of Engineering, Nagoya University, Japan. A special appreciation should be given to Prof. H. Takahashi, Department of Mechanical System Engineering, School of Engineering, Yamagata University, Japan, for providing the original FEPM sourcing code. One of the authors (L. Q. CHEN) would like to thank Dr. M. Kobashi and Dr. T. Itoh in this laboratory for providing much assistance during his stay in Japan.

REFERENCES

[1] Spitzig W A, Pelton A R, Laabs F C. Characterization of the strength and microstructure of heavily cold worked Cu-Nb composites[J]. Acta Metall, 1987, 35(10): 2427-2442.

[2] Spitzig W A, Krotz P D. Comparison of the strengths and microstructures of Cu-20% Ta and Cu-20% Nb in situ composites[J]. Acta Metall, 1988, 36(7): 1709-1715.

[3] Hong S I, Hill M A. Mechanical properties of Cu-Nb microcomposites fabricated by the bundling and drawing process[J]. Scripta Mater, 2000, 42(8): 737-742.

[4] Russell A M, Lund T, Chumbley L S, et al. A high-strength, high-conductivity Al-Ti deformation processed metal-metal matrix composite[J]. Composites, Part A: Applied Science and Manufacturing, 1999, 30(3): 239-247.

[5] Xu K, Russell A M, Chumbley L S, et al. A deforma-

tion processed Al-20% Sn in situ composite[J]. Scripta Mater, 2001, 44(6): 935-940.

[6] Raabe D, Mattissen D. Microstructure and mechanical properties of a cast and wire-drawn ternary Cu-Ag-Nb in situ composite[J]. Acta Mater, 1998, 46(16): 5973-5984.

[7] Thilly L, Véron M, Ludwig O, et al. Deformation mechanism in high strength Cu/Nb nanocomposites [J]. Mater Sci Eng, 2001, A309-310: 510-513.

[8] Chen L Q, Kanetake N. Fabrication and mechanical behavior of powder metallurgy processed in situ Nb/Al sheet metal-metal composites[J]. Mater Sci Eng, 2004, A 367(1-2): 295-300.

[9] Chen L Q, Kanetake N. Textures in a powder metallurgy processed Nb/Al Composites[J]. Mater Sci Forum, 2002, 408-412: 1765-1770.

[10] Chen L Q, Kanetake N. Hot-extruded and cold-rolled textures of the matrix aluminum in deformation processed two-phase Nb/Al metal-metal composites[J]. Textures and Microstructures, 2003, 35(3-4): 283-292.

[11] Mathur K K, Dawson P R. On modeling the development of crystallographic texture in bulk forming processes[J]. Int J Plasticity, 1989, 5(1): 67-94.

[12] Kalidindi S R, Anand L. An approximate procedure for predicting the evolution of crystallographic texture in bulk deformation processing of fcc metals[J]. Int J Mech Sci, 1992, 34(4): 309-329.

[13] Schoenfeld S E, Asaro R J. Through thickness texture gradients in rolled polycrystalline alloys[J]. Int J Mech Sci, 1996, 38(6): 661-683.

[14] Takahashi H, Saitoh T, Motohashi H, et al. Prediction of plastic anisotropy in aluminium sheet by finite-element polycrystal model (1st Report, Finite-element polycrystal model)[J]. Trans of Japan Soc of Mech Engineers, 1994, 60(4): 1017-1022.

[15] Takahashi H, Mashiko M, Motohashi H, et al. Prediction of plastic anisotropy in aluminium sheet by finite-element polycrystal model (2nd Report, Prediction of plastic anisotropy in rolled sheet)[J]. Trans of Japan Soc of Mech Engineers, 1994, 60(5): 1210-1215.

[16] Takahashi H. Numerical material testing and plastic working analysis using finite element polycrystal model[J]. J Japan Soc Tech Plasticity, 1996, 37(12): 1244-1251.

[17] Takahashi H. Polycrystal Plasticity[M]. Tokyo: Corona Publishing Co Ltd, 1999. 56.

[18] Humphreys F J. The thermomechanical processing of Al-SiC particulate composites[J]. Mater Sci Eng, 1991, A135: 267-273.

[19] Chen L Q, Kanetake N. Simulation of the rolling textures in Nb/Al composites with finite element polycrystal model[A]. Proceedings of the 2002 Japanese Spring Conference for the Technology of Plasticity [C]. Chiba, Japan, 2002. 415-416.

(Edited by YANG Bing)